THE JOURNAL OF PHYSICAL CHEMISTRY B

Article

pubs.acs.org/JPCB

Dynamical Features in Cationic Micelles of Varied Chain Length

V. K. Sharma,[†] S. Mitra,[†] V. Garcia Sakai,[‡] and R. Mukhopadhyay*,[†]

[†]Solid State Physics Division, Bhabha Atomic Research Centre, Mumbai 400085, India

[‡]ISIS Facility, Science and Technology Facilities Council, Rutherford Appleton Laboratory, Didcot OX11 0QX, U.K.

ABSTRACT: Chain length is one of the parameters controlling the structural arrangement of micelle monomers, such that one can tailor the monomers for different applications, but the effect of chain length on the dynamical behavior of micelles is unknown. In this article, we report a study on the effect of varying chain length on the dynamical behavior of alkyltrimethylammonium bromide (C_nTAB) micelles (n = 10, 12, 14, and 16) using incoherent quasielastic neutron scattering (QENS). The data analysis clearly shows the presence of two distinct motions: global motion of whole micelles and faster internal motions of the C_nTAB monomers. The global diffusion is Fickian in nature, whereas the internal motions can be described with a model that considers the motions of the headgroup and the hydrophobic alkyl chain separately. Methyl groups in the headgroup undergo 3-fold jump rotations, and the hydrogen atoms belonging to the alkyl chain undergo localized translational diffusion. The hydrogen atoms belonging to the alkyl chain are confined within spherical volumes that increase linearly along the C_nTAB chain: the hydrogen atoms closer to the headgroup move within smaller spheres with lower diffusion coefficients than those farther from the headgroup. The main result is that, with increasing chain length, the dynamics of the C_nTAB monomer is greatly affected: diffusion is reduced and occurs in smaller spheres, and residence times are increased. Global motion is also hindered with increased chain length.

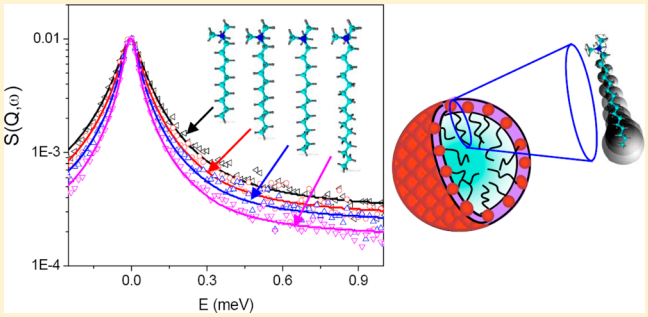

INTRODUCTION

Surfactants are among the most versatile products in chemistry from the points of view of both their interesting properties and their applications; therefore, it is not surprising that they are being investigated extensively. Surfactants have a wide range of applications, for example, in the pharmaceutical, medical, and food industries and for material synthesis.[1−3] In aqueous solutions at concentrations above the critical micellar concentration (CMC), surfactant molecules are known to self-aggregate to form micelles. The CMC depends on various parameters such as the size of the headgroup, the length of the hydrophobic tail, and the temperature. Micelle formation results from the delicate balance between two opposing forces, namely, the attractive hydrophobic interaction of the tails and the ionic or steric repulsion of the head groups. The attractive tail−tail hydrophobic interaction provides the driving force for the aggregation of surfactant molecules, whereas the electrostatic repulsion between the headgroup puts a lower limit on the size that a micelle can attain. The surfactant molecules adopt a preferential orientation with their hydrophilic headgroups pointing toward the aqueous phase and their hydrophobic tails pointing away from it. By tailoring the architecture of the surfactant molecules and the interaction between them, discrete micellar structures of a specific size, shape, and order can be created. Here, our interest is in an important class of cationic micelles, the n-alkyltrimethylammonium bromides $[C_nH_{2n+1}N(CH_3)_3Br$ (C_nTAB) for n = 10, 12, 14, and 16). C_nTAB is commonly used in a variety of applications: in hair-drying products, in the extraction of DNA, and in the synthesis of gold nanoparticles, for example. C_nTAB surfactant molecules ionize in aqueous solution, and the corresponding micelles are aggregates of C_nTA^+ ions. The micelle is positively charged and is thus called a cationic micelle. The Br^- ions, known as counterions, tend to stay near the C_nTA^+ micellar surface, as shown in Figure 1. The counterions located at short enough

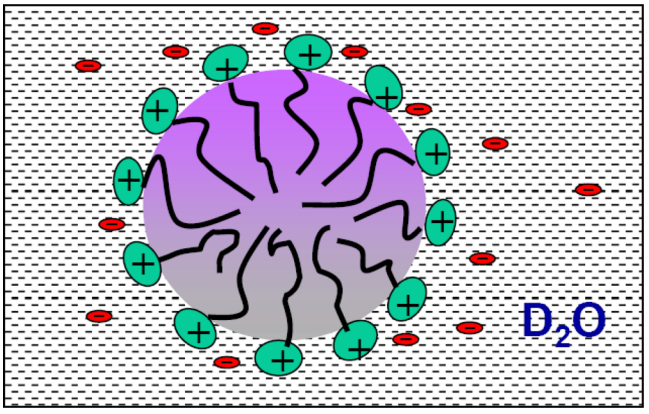

Figure 1. Schematic of a cationic micellar solution in D_2O.

Received: May 18, 2012
Revised: July 4, 2012
Published: July 9, 2012

   dx.doi.org/10.1021/jp304841a | J. Phys. Chem. B 2012, 116, 9007−9015

distances from the micellar surface feel a very strong electrostatic attraction compared with the thermal energy, and these counterions are referred to as "bound to" or "condensed on" the micelles.[4] In ionic micellar solutions, counterion condensation determines the effective charge on the micelles and hence the formation, structure, and interaction of the micelles. Counterion condensation can be varied by changing the chain length of the surfactant or the temperature or by adding electrolytes, among other methods. The effect of changing the hydrocarbon chain length on the structure of C_nTAB micelles has been studied very well using small-angle neutron scattering.[4−6] Micellar properties such as size/shape, aggregation number, fractional charge, and CMC have been found to be affected by chain length.

The aggregation number and size of C_nTAB micelles increase with the length of the hydrocarbon chain, whereas the CMC decreases because the larger hydrophobic part of the surfactant molecule favors micellization.[5,6] Berr[5] showed that, for a 0.1 M micellar solution of C_nTAB, micelles of C_{12}TAB and C_{14}TAB are more or less spherical whereas, for monomers with higher n values, such as C_{16}TAB, at the same concentration and temperature, a more pronounced prolate ellipsoidal shape is better able to accommodate the extra hydrocarbons in the core.[5] The micelles appear to become drier, in terms of both water content and depth of water penetration, as the chain length n increases. The fractional charge of micelles decreases with the alkyl-chain length.[5,6] Although the structures (sizes and shapes) of C_nTAB micelles with varied chain length have been studied extensively,[4,6] no information is available on the effects of chain length on the dynamical aspects of these micelles. Therefore, it is of interest to investigate this issue to establish any correlation that might exist between the dynamical behavior and the microstructure of the micelles. Local dynamics of such assemblies are important in understanding various properties such as the mechanism in releasing solubilized drugs and the micellar breaking time. Internal motions in micelles can be studied experimentally using various techniques such as nuclear magnetic resonance (NMR) spectroscopy,[7−12] Raman scattering,[13,14] and neutron scattering.[15−23] NMR examination of micellar solutions shows the existence of two types of motion:[10] Whereas slower motion on the nanosecond time scale is related to micellar tumbling and surfactant lateral diffusion along the micellar surface, faster motion on the picosecond time scale corresponds to the internal motions of alkyl chain within the micelles.[10] The vibrational dynamics of micellar assemblies have also been probed using Raman spectroscopy.[13,14] The characteristic vibrational bands, their frequency positions, their widths, and the peak-height ratios of selected bands were found to be very sensitive to external parameters such as temperature, pressure, and electrolyte concentration. Pressure-induced phase transitions of C_{14}TAB micellar solutions studied by Raman spectroscopy have been reported,[13] where increasing pressure was found to lead to an increase in the trans conformation and, hence, to ordering of the surfactants. A similar effect was observed upon lowering of the temperature of the micellar solution. Neutron scattering, in particular, the quasielastic neutron scattering (QENS) technique, has considerable potential to provide insight into the internal dynamics of micelles.[16−21] The internal dynamics of sodium bis(2-ethylhexyl) sulfosuccinate (AOT) reverse micelles in deuterated cyclohexane (C_6D_{12}) have been studied as a function of hydration: In the anhydrous case, the observed quasielastic broadening was attributed entirely to the global motion of the AOT reverse micelles. However, when the hydration was increased above a certain threshold, the onset of internal motion of the micelles was observed along with the global motion.[16] For block copolymer micelles, Castelletto et al.[17] observed two dynamical modes, namely, fast and slow modes. The slow mode that dominates at low scattering angle corresponds to the translational diffusion of micelles, whereas the fast mode is due to internal motions of the micelles. Previously, we studied the dynamics of sodium dodecyl sulfate (SDS) based micelles, in detail, using the QENS technique.[18−20] We observed two distinct motions: (i) global motion of entire micelles and (ii) internal motions of monomers. The global motion was found to be Fickian in nature. The internal motions of the SDS monomers was described by a model in which hydrogen atoms undergo localized translational motions. Molecular dynamics (MD) simulations have been quite successful in complementing experimental techniques in the study of the dynamics of micelles.[24−26] MD simulations of SDS and sodium dodecylbenzene sulfonate (SDBS) micelles[25] showed that the tail ends of the hydrocarbon chains exhibit larger segmental mobility than the higher parts of the chain, consistent with our QENS experimental results.[18]

Herein, we report a systematic QENS study on a series n-alkyltrimethyl ammonium bromides micelles (C_nTAB with n = 10, 12, 14, and 16). All other factors that could affect the dynamics, such as the molar concentration of the surfactant and temperature, were kept constant such that effects of chain length alone on the dynamics could be probed. In this article, we show that the experimental data observed from a series of C_nTAB micelles is well described by a quantitative model that takes into account the nature of internal motions. The effects of chain length on the observed dynamics are also discussed in detail.

EXPERIMENTAL DETAILS

All C_nTAB cationic surfactants (n = 10, 12, 14, and 16) were obtained from Aldrich. For all of the C_nTAB surfactants, 0.3 M micellar solutions were prepared separately by dissolving C_nTAB in D_2O (99.9% atom D purity). Neutron scattering experiments were carried out using the inverted geometry spectrometer IRIS at the ISIS pulsed neutron source (Didcot, U.K.). IRIS was operated with a 002 pyrolytic graphite analyzer, providing and energy resolution of $\Delta E \approx 17.5$ μeV (full width at half-maximum, fwhm) and with an energy transfer range from −0.3 to 1.2 meV (in the offset mode). The wave-vector transfer ($\mathbf{Q}$) range covered was 0.5−1.8 Å^{-1}. Measurements were carried out on a series of C_nTAB systems, namely, C_{10}TAB, C_{12}TAB, C_{14}TAB, and C_{16}TAB. Data were also recorded for pure D_2O. To study the effect of temperature, data were recorded at 300, 315, and 330 K. The samples were placed in an annular aluminum can with an internal spacing of 1 mm to minimize multiple scattering and obtain reasonable measuring statistics. The ISIS data analysis package MODES[29] was used to carry out data reduction involving background subtraction, detector efficiency corrections, and so on.

DATA ANALYSIS

In a neutron scattering experiment, the measured intensity is proportional to the double-differential cross section[15]

dx.doi.org/10.1021/jp304841a | J. Phys. Chem. B 2012, 116, 9007−9015

$$\frac{\partial^2\sigma}{\partial\omega\partial\Omega} = \frac{\mathbf{k}}{\mathbf{k_0}}[\sigma^{coh}S^{coh}(\mathbf{Q}, \omega) + \sigma^{inc}S^{inc}(\mathbf{Q}, \omega)] \quad (1)$$

where $S(\mathbf{Q},\omega)$ is known as the scattering law and the superscripts coh and inc denote the coherent and incoherent components, respectively. $\mathbf{k}$ and $\mathbf{k}_0$ are the final and initial wave vectors, respectively. Micellar systems mainly contain protons, which have a large incoherent neutron scattering cross section (80 barns, compared to a coherent part of 1.7 barns and compared to the total scattering cross sections of other elements in the monomer: 5.5 barns for C atoms and 4.2 barns for O atoms). Therefore, in a neutron scattering experiment from micelles, the observed dynamics mainly corresponds to the self-correlation function of the protons $S(\mathbf{Q},\omega) = S^{inc}(\mathbf{Q},\omega)$. Specifically for the system under study here, we are interested in the dynamics of hydrogenated micelles in solution, and therefore, we used deuterated water to minimize the scattering contribution from the solvent. Spectra from the pure solvent were recorded and subtracted from those measured for the micellar solutions, rather than being modeled with a separate scattering function. To minimize systematic errors, the measurements were performed in the same sample cell first for D_2O and then for a micellar solution. Both spectra were normalized to monitor counts, and the final scattered intensity from the micelles was obtained using the relation

$$\phi I_{micelles}(Q, \omega) = I_{solution}(Q, \omega) - (1 - \phi)I_{D_2O}(Q, \omega) \quad (2)$$

where ϕ is the volume fraction of C_nTAB in the D_2O. The factor ϕ accounts for the fact that the amount of D_2O in a micellar solution is less than that measured in the pure D_2O sample.

Micelles in solution have the freedom to undergo a variety of motions including whole-body translational diffusion and rotation and internal motions within the micelle corresponding to the dynamics of the individual monomers.[18−20] To interpret the data we assumed that these dynamical processes are independent of each other, such that the Q-averaged scattering law $S_{micelles}(Q,\omega)$ can be expressed as

$$S_{micelles}(Q, \omega) = [S_{trans}(Q, \omega) \otimes S_{rot}(Q, \omega) \otimes S_{internal}(Q, \omega)] \quad (3)$$

where $S_{trans}(Q,\omega)$, $S_{rot}(Q,\omega)$, and $S_{internal}(Q,\omega)$ correspond to the scattering functions due to translation, rotation, and internal motions, respectively, of the micelles.

It has been shown that the combination of independent translational and rotational motions of a dense hard-sphere particle can be well approximated by a single Lorentzian.[27] It was shown that rotational diffusion does not modify the essential Lorentzian shape of the scattering function as assumed for translational motion or its Q variation, but it does increase its width, leading to an apparent diffusion coefficient slightly higher than D_S (the self-diffusion coefficient for pure translational motion).[27] This approximation is certainly helpful because considering both translational and rotational motions explicitly would increase the complexity of the data analysis. This methodology has been used to describe the dynamical motion in various aggregates such as micelles,[18,19] reverse micelles,[16] and proteins.[27] Therefore, the scattering law for global motion considering both translation and rotation can be expressed as

$$\begin{aligned} S_G(Q, \omega) &= S_{trans}(Q, \omega) \otimes S_{rot}(Q, \omega) \\ &= L_G(\Gamma_G, \omega) \\ &= \frac{1}{\pi}\frac{\Gamma_G}{\Gamma_G^2 + \omega^2} \end{aligned} \quad (4)$$

where Γ_G is the half-width at half-maximum of the Lorentzian corresponding to global motion.

Internal motions of micelles correspond to the motion of the monomers where the scatterers are confined within a certain volume of space. At long times, there is a finite probability of finding the scatterer within this volume. This gives rise to an elastic contribution to the scattering law, $S_{internal}(Q,\omega)$. Therefore, the scattering law for $S_{internal}(Q,\omega)$ can be expressed as

$$S_{internal}(Q, \omega) = A(Q)\,\delta(\omega) + [1 - A(Q)]L_{in}(\Gamma_{in}, \omega) \quad (5)$$

where the elastic part, $A(Q)\,\delta(\omega)$, arises due to motion slower than the longest observable time as determined by the energy resolution of spectrometer. The second term in eq 5 represents the quasielastic component, which was approximated as a single Lorentzian function, $L_{in}(\Gamma_{in},\omega)$, with a half-width at half-maximum (hwhm), Γ_{in}, that is inversely proportional to the time scale of motion. The contribution of the elastic scattering to the total scattering spectrum is called the elastic incoherent structure factor (EISF). Therefore, $A(Q)$ in eq 5 is simply the EISF, which represents the space Fourier transform of the particle distribution, taken at infinite time and averaged over all possible initial positions. Therefore, combining these dynamical processes leads to the scattering law for micelles, which can be written as

$$\begin{aligned} S_{micelles}(Q, \omega) &= L_G(\Gamma_G, \omega) \otimes \{A(Q)\,\delta(\omega) \\ &\quad + [1 - A(Q)]L_{in}(\Gamma_{in}, \omega)\} \\ &= A(Q)\,L_G(\Gamma_G, \omega) + [1 - A(Q)]L_{tot} \\ &\quad (\Gamma_{tot}, \omega) \end{aligned} \quad (6)$$

Here, the Lorentzian $L_G(\Gamma_G,\omega)$ corresponds to the global motion of the whole micelle and the Lorentzian $L_{tot}(\Gamma_{tot},\omega)$ represents the combination of global micellar motion and internal motions of the micelle, where $\Gamma_{tot} = \Gamma_G + \Gamma_{in}$. Equation 6, convoluted with the instrumental resolution, was used to describe the QENS data corresponding to the micelles. A least-squares fitting method was used to fit the spectra with the parameters $A(Q)$, Γ_G, and Γ_{tot}. No a priori model for the Q dependence was introduced into the fit, for either the weight factor or the hwhm values of the Lorentzian functions. Therefore, the behavior of the fit parameters can be used to verify different theoretical models. The QENS data were analyzed using the program DAVE[30] developed at the NIST Center for Neutron Research.

RESULTS AND DISCUSSION

Scattering functions for the micelles, $S_{micelles}(Q,\omega)$, were obtained by subtracting the contribution of D_2O from the micellar solution using eqs 1 and 2 and are shown in Figure 2a, where the spectra have been normalized to the peak intensities. The instrumental resolution, as measured using a standard vanadium sample, is also shown for comparison. It is evident that all of the C_nTAB micelles exhibit significant quasielastic broadening over the instrumental resolution. It is evident from

dx.doi.org/10.1021/jp304841a | J. Phys. Chem. B 2012, 116, 9007−9015

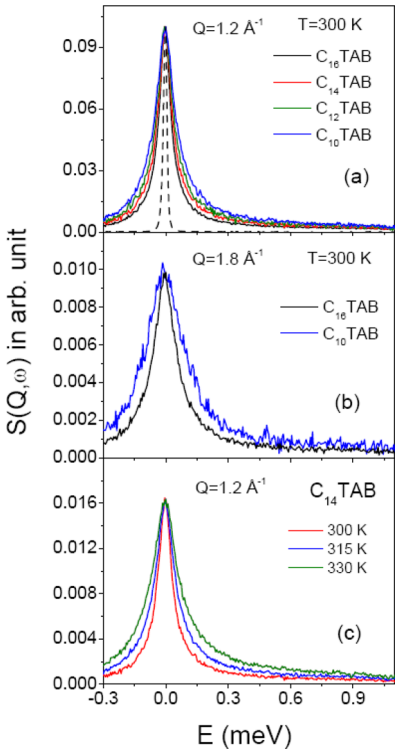

Figure 2. Typical QENS spectra for 0.3 M C_nTAB micellar solutions: (a) for different chain lengths at aa typical value of $Q = 1.2$ Å^{-1}, (b) for C_{10}TAB and C_{16}TAB micelles at $Q = 1.8$ Å^{-1}, (c) for C_{14}TAB micelles at $Q = 1.2$ Å^{-1} at different temperatures. All spectra are normalized to peak intensity. The instrument resolution is shown by the dashed line.

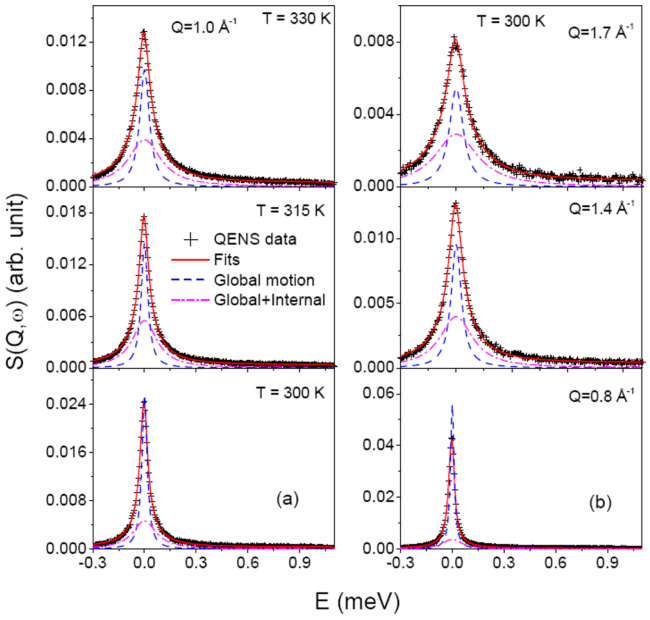

Figure 3. Typical fitted $S_{micelles}(Q,\omega)$ data for 0.3 M C_{14}TAB micelles (a) for different temperatures at $Q = 1.0$ Å^{-1} and (b) for different Q values at $T = 300$ K, assuming the model function given in eq 6.

Figure 2a that the quasielastic (QE) broadening was greatest for the micelle with the smallest chain length, C_{10}TAB. This broadening decreased with increasing chain length and reached a minimum for the micelle with the longest chain, C_{16}TAB. This difference in QE broadening was more pronounced at high wave vector transfer Q. The peak normalized QENS spectra for C_{10}TAB and C_{16}TAB micelles at $Q = 1.8$ Å^{-1} are shown in Figure 2b. The effect of temperature on the QENS spectra for C_{14}TAB micelles is also shown in Figure 2c. As expected, QE broadening increased with increasing temperature.

For data analysis, the model scattering law (eq 6) was convoluted with the instrumental resolution function, and the parameters involved [$A(Q)$, Γ_G, and Γ_{tot}) were obtained by least-squares fitting of the experimental data. Typical fitted spectra for the C_{14}TAB micelles at different temperatures are shown in Figure 3a for $Q = 1.0$ Å^{-1}. It is evident from the figure that the hwhm values of both Lorentzian functions and the relative area of the broader one increased with the temperature. Figure 3b shows typical fitted spectra for C_{14}TAB micelles at different Q values at 300 K. For all of the C_nTAB micelles, typical fitted spectra at a particular value of $Q = 1.2$ Å^{-1} are shown in Figure 4. It is clear from Figure 4 that the relative area of the narrower Lorentzian increased with the chain length. It is evident that the model scattering law (eq 6) describes the data very well for all of the C_nTAB micelles at different temperatures and Q values. To gain more insight into the nature of these two dynamical processes, global and internal, the parameters obtained from the fit were analyzed as functions of Q. It can be expected that the global motion of the whole C_nTAB micelle is slower than the internal motions, as observed in our earlier study on the SDS micelles.[18,19] Therefore, it can be assumed that the slower global motion corresponds to the narrower Lorentzian (hereafter referred to as the first Lorentzian), whereas the broader Lorentzian (hereafter referred to as the second Lorentzian), which represents the convolution of two Lorentzians, corresponds to both global and internal motions of the micelles.

Global Motion. The variation with Q^2 of the hwhm, Γ_G, of the first Lorentzian, corresponding to the global dynamics of the micelles, for different C_nTAB micellar systems is shown in Figure 5. A simple Brownian motion following Ficks law, $\Gamma_G = D_G Q^2$, was found to describe the observed behavior quite well. Here, D_G is the diffusion coefficient corresponding to the global motion. For each C_nTAB micellar system, D_G was obtained from the slope of a plot of Γ_G versus Q^2. For example, D_G for C_{14}TAB micelles was found to be 2.5×10^{-6} cm^2/s at 300 K. Obtained values of global diffusion coefficients can be compared with those of other macromolecules (micelles, proteins, etc.). For example, the reported global diffusion coefficient of SDS micelles at 300 K is $(2.5 \pm 0.1) \times 10^{-6}$ cm^2/s.[18] For apo-calmodulin protein, the global diffusivity was found to be 2.5×10^{-6} cm^2/s at 323 K.[28] The global diffusion coefficients of myoglobin and lysozyme proteins were found to be $(8.2 \pm 0.2) \times 10^{-7}$ and $(9.1 \pm 0.2) \times 10^{-7}$ cm^2/s, respectively, at 298 K.[27] The global diffusivity for C_nTAB micelles was found to be higher than those of the reported proteins, which might be due to the difference in the hydrodynamic size between proteins and micellar aggregates. It can be noted here that D_G is an apparent global diffusion coefficient, which is slightly higher than D_S (the self-diffusion constant for pure translational motion of the micelles), which can be obtained directly from the Stokes–Einstein relation $D_S = k_B T/6\pi\eta R$, where R is the hydrodynamic radius of the micelles, η is the viscosity of D_2O, and T is the temperature of the solution. For a micelle of radius $R \approx 20$ Å, the estimated self-diffusion coefficient is $\sim 1.2 \times 10^{-6}$ cm^2/s at 300 K ($\eta = 0.9$

dx.doi.org/10.1021/jp304841a | J. Phys. Chem. B 2012, 116, 9007–9015

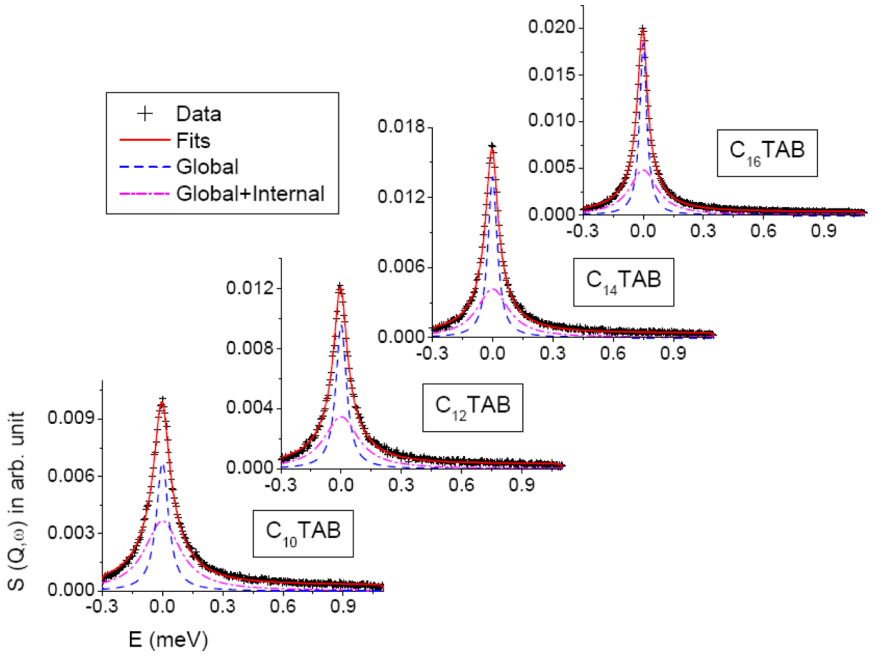

Figure 4. Typical fitted $S_{micelles}(Q,\omega)$ data for 0.3 M C_nTAB micellar solution at a typical value of Q = 1.2 Å^{-1} assuming the model function given in eq 6.

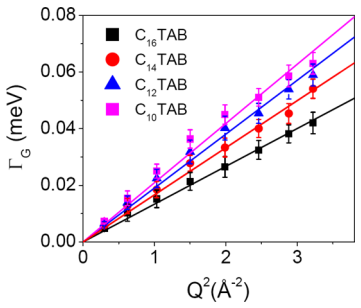

Figure 5. Variation with Q^2 of the half-width at half-maximum, Γ_G, of the Lorentzian $L_G(\Gamma_G,\omega)$, corresponding to the global motion of C_nTAB micelles (n = 10, 12, 14, and 16) at 300 K. The solid lines correspond to fits with Fick's law of diffusion.

cP[17] for D_2O at 300 K), which is half of that obtained from the QENS data.

The variation of the obtained D_G values for C_nTAB micelles with different chain lengths at 300 K is shown in Figure 6. D_G values obtained for C_{14}TAB micelles at different temperatures are also shown in Figure 6. It is evident that the diffusivity

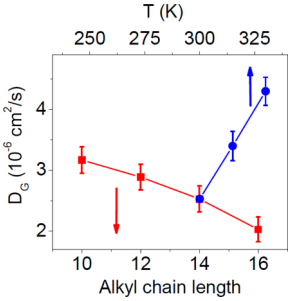

Figure 6. Variation with alkyl-chain length of the global diffusivity, D_G, for different C_nTAB micelles at 300 K. The temperature dependence of D_G for C_{14}TAB is also shown.

corresponding to the global motion of the C_nTAB micelles decreases with increasing monomer chain length. For C_{10}TAB micelles, D_G = 3.2 × 10^{-6} cm^2/s was obtained, whereas for C_{16}TAB micelles, D_G was found to be equal to 2.0 × 10^{-6} cm^2/s. It can be noted that small-angle neutron scattering and NMR data on C_nTAB micelles showed that the aggregation number and size of the micelles increase with increasing alkyl-chain length.[4−7] Berr[5] found the values of the minor and major axes to be 21.9 and 26.1 Å, respectively, for 0.1 M C_{12}TAB micelles and to increase to 26.6 and 44.3 Å, respectively, for 0.1 M C_{16}TAB micelles. The aggregation number was found to increase from 50 to 164 from C_{12}TAB to C_{16}TAB micelles. The available structural parameters are listed in Table 1. The

Table 1. Various Shape- and Size-Related Parameters for 0.1 M C_nTAB Micelles of Different Chain Lengths As Obtained Using Small-Angle Neutron Scattering (SANS) at 298 K[5]

micelle	aggregation number	micellar charge Z (+)	fractional charge $\beta = Z/N$ (+)	minor axis A_T (Å)	major axis B_T (Å)	axial ratio
C_{12}TAB	50	15	0.31	21.9	26.1	1.19
C_{14}TAB	84	19	0.23	25.7	29.6	1.15
C_{16}TAB	163	23	0.14	26.6	44.3	1.66

decrease in global diffusivity with increasing chain length as observed here is a manifestation of the combined effects of the increases in hydrodynamic size and aggregation number of the micelles. Figure 6 shows that the D_G value of C_{14}TAB micelles increased with temperature, as expected for a thermally activated diffusive motion.

Internal Motion. As mentioned previously, the QENS data indicated presence of two Lorentzian functions (eq 6): (i) The first one corresponds to global motion as discussed in the preceding section, and (ii) the second Lorentzian has contributions from both internal and global motions, as expressed in eq 6. The width of the second Lorentzian (Γ_{tot}) is the sum of the widths of the Lorentzians for the global (Γ_G)

dx.doi.org/10.1021/jp304841a | J. Phys. Chem. B 2012, 116, 9007−9015

and internal (Γ_{in}) motions. As Γ_G is already known, Γ_{in} was obtained by subtracting Γ_G from Γ_{tot}. To investigate the nature of the internal motions, the parameters Γ_{in} and EISF $[A(Q)]$ were analyzed as functions of Q. The variation of EISF with Q for different C_nTAB micellar solutions at 300 K is shown in Figure 7.

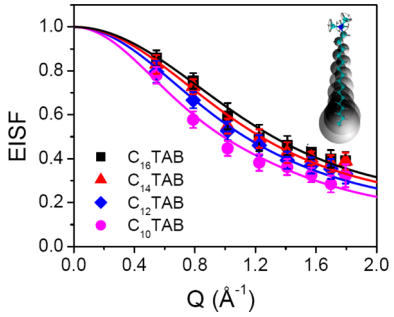

Figure 7. Variation of EISF for C_nTAB micelles (n = 10, 12, 14, and 16) at 300 K. Solid lines represent calculated EISFs for the model described in the text. Inset: Schematic of the proposed model.

As mentioned earlier, C_nTAB surfactants consist of a headgroup, containing three methyl groups, and a long alkyl chain with n carbon atoms. Therefore, apart from the dynamics of the chain, the dynamics of the headgroup can also contribute to the internal motions of the monomer. For C_nTAB molecules with different chain lengths, the structure of the headgroup is the same, and only the number of CH_2 units in the alkyl chain changes. The dynamics of the methyl hydrogen atoms in the headgroup can be modeled by a 3-fold jump rotation in which the hydrogen atoms reorient by 120° jumps on a circle about the 3-fold symmetry axis. The scattering law, $S^{3\text{-fold}}(Q,\omega)$ for the same can be found in ref 14.

For the alkyl-chain dynamics, which involves the bending and stretching modes of chemical bonds, the reorientation of the alkyl chain, and so on, these motions can be effectively modeled considering that the hydrogen atoms of each CH_2 unit undergo diffusion limited within a sphere. For a long alkyl-chain system, the flexibility of the chain demands that the hydrogen atoms at different positions along the chain move in spheres having different radii and diffusivities.[18,19] Different distribution functions for the radii and diffusivities can be considered, including linear, Gaussian, and log-normal, among others.[18,19,23,28,31] We employed a simple linear distribution similar to that used for modeling alkyl chains in dicopper tetrapalmitate,[31] phospholipid liposomes,[23] and SDS micelles,[18] that we found to be more suitable for our system than the log-normal distribution used to describe the internal motions in the more complex system of the apo-calmodulin protein.[28] This model seems more appropriate because it takes into account the fact that different protons along the C_nTAB chains undergo diffusive motion over significantly different spatial extents. Therefore, the scattering law for alkyl-chain motion can be written as[18,32]

$$S_{\text{alkyl chain}}(Q,\omega) = \frac{1}{n}\sum_{i=1}^{n}\left\{A_0^0(QR_i)\,\delta(\omega) + \frac{1}{\pi}\sum_{\{l,m\}\neq\{0,0\}}(2l+1)A_m^l(QR_i)\,\frac{(x_m^l)^2 D_i/R_i^2}{[(x_m^l)^2 D_i/R_i^2]^2+\omega^2}\right\} \quad (7)$$

In eq 7, $A_0^0(QR_i) = \{[3j_1(QR_i)]/(QR_i)\}^2$ is the elastic structure factor, where j_1 is the first-order spherical Bessel function. The second term in eq 7 is the quasielastic component, which comprises a series of Lorentzians. $A_m^l(QR_i)$ $(m, l \neq 0, 0)$ are the quasielastic structure factors and can be calculated for different m and l values using the values of x_m^l listed in ref 32. R_i and D_i are the radius of the sphere and the associated diffusivity, respectively, at the ith site of the alkyl chain from the head toward the tail and can be written as

$$R_i = \frac{i-1}{n-1}(R_{\max} - R_{\min}) + R_{\min} \quad (8)$$

and

$$D_i = \frac{i-1}{n-1}(D_{\max} - D_{\min}) + D_{\min} \quad (9)$$

where n is total number of carbon atoms in the alkyl chains of the C_nTAB monomer. Based on this model, the hydrogen atoms of the first (i = 1) CH_2 unit (nearest the headgroup) will move within the smallest sphere of radius R_{min} and with the minimum diffusion coefficient D_{min}. Moving away from the headgroup along the alkyl chain, both the diffusivity and the radius of the sphere increase, and the hydrogen atoms at the end of the tail (i.e., farthest from the headgroup) will generate the largest sphere of radius R_{max} with the maximum diffusion coefficient D_{max}. NMR spectral investigations and fluorescence decay measurements of micellar solutions have also shown that the mobility of the chains increases from the polar head to the nonpolar tail.[9,11,12] It has been shown that the correlation time and the order parameter corresponding to the tail end of the hydrocarbon chain are smaller than those corresponding to the end near the headgroup. Furthermore, recent molecular dynamics simulations of micelles also suggest that the tail end is more flexible than the end near the headgroup.[25]

Therefore, the resultant scattering function for the segmental motion of C_nTAB monomers can be expressed as a combination of scattering functions arising from the motion of the headgroup (3-fold rotation) and the motions of the alkyl chain (diffusion within spheres) weighted by the number of hydrogen atoms in the head and chain groups. This scattering law can be written as

dx.doi.org/10.1021/jp304841a | J. Phys. Chem. B 2012, 116, 9007−9015

Table 2. Radii of Spheres, R_{min} and R_{max}, and Associated Diffusion Coefficients, D_{min} and D_{max}, for Hydrocarbon Chains and Mean Residence Times (τ) for Hydrogen Atoms in the Head Group, As Obtained from Least-Squares Fitting of the Data (Figures 7 and 8) with the Model Discussed in the Text for C_nTAB Molecules with Different Chain Lengths n

micelle	T (K)	R_{min} (Å)	R_{max} (Å)	D_{min} (10^{-5} cm^2/s)	D_{max} (10^{-5} cm^2/s)	τ (ps)
C_{10}TAB	300	0.10 ± 0.03	4.4 ± 0.3	0.30 ± 0.06	1.6 ± 0.2	2.6 ± 0.2
C_{12}TAB	300	0.04 ± 0.02	3.5 ± 0.3	0.15 ± 0.03	1.3 ± 0.2	4.0 ± 0.3
C_{14}TAB	300	0.02 ± 0.01	3.1 ± 0.2	0.08 ± 0.02	1.1 ± 0.2	4.8 ± 0.4
	315	0.40 ± 0.08	4.4 ± 0.3	0.15 ± 0.04	1.6 ± 0.2	4.1 ± 0.3
	330	0.50 ± 0.09	4.8 ± 0.4	0.23 ± 0.05	2.3 ± 0.3	3.6 ± 0.3
C_{16}TAB	300	0.02 ± 0.01	2.8 ± 0.2	0.1 ± 0.04	1.0 ± 0.2	6.5 ± 0.6

$$S_{internal}(Q,\omega) = P_h S^{3\text{-fold}}(Q,\omega) + P_t \frac{1}{n} \sum_{i=1}^{n} \left\{ A_0^0(QR_i)\,\delta(\omega) + \frac{1}{\pi} \sum_{\{l,m\}\neq\{0,0\}} (2l+1) A_m^l(QR_i) \frac{(x_m^l)^2 D_i/R_i^2}{[(x_m^l)^2 D_i/R_i^2]^2 + \omega^2} \right\} \quad (10)$$

where P_h and P_t are the fractions of hydrogen atoms in the headgroup and alkyl chain, respectively. For C_nTAB molecules, $[C_nH_{2n+1}N^+(CH_3)_3Br^-]$, P_h and P_t are equal to $9/(2n+10)$ and $(2n+1)/(2n+10)$, respectively. In eq 10, the first term corresponds to the motion of hydrogen atoms belonging to the headgroup, and second term represents those of hydrogen atoms in the alkyl chain. Rearrangement of the various terms in eq 10 leads to the equation

$$S_{internal}(Q,\omega) = \left[P_h B_0(Qa) + \frac{P_t}{n} \sum_{i=1}^{n} A_0^0(QR_i) \right] \delta(\omega) + \frac{1}{\pi} \left(P_h B_1(Qa) \frac{3\tau}{9+\omega^2\tau^2} + \frac{P_t}{n} \sum_{i=1}^{n} \sum_{\{l,m\}\neq\{0,0\}} \left\{ (2l+1) A_m^l(QR_i) \frac{(x_m^l)^2 D_i/R_i^2}{[(x_m^l)^2 D_i/R_i^2]^2 + \omega^2} \right\} \right) \quad (11)$$

where $B_0(Qa) = {}^1/_3[1 + 2j_0(Qa)]$ and $B_1(Qa) = {}^2/_3[1 - j_0(Qa)]$ are the elastic and quasielastic structure factors, respectively, in the scattering law for 3-fold jump rotation and j_0 is the zeroth-order spherical Bessel function. a is the distance between two hydrogen atoms in a methyl group (1.8 Å), and τ is the mean residence time at each site during 3-fold jump rotation. Therefore, the EISF corresponding to the internal motion of the C_nTAB monomer can be written as

$$A(Q) = \frac{1}{(2n+10)} \left\{ \frac{9}{3}[1 + 2j_0(Qa)] + (2n+1)\frac{1}{n} \sum_{i=1}^{n} \left[\frac{3j_1(QR_i)}{QR_i} \right]^2 \right\} \quad (12)$$

R_{min} and R_{max} were determined by least-squares fitting of the extracted EISF data as described in eqs 12 and 8. The solid lines in Figure 7 represent the resulting fits. The values of R_{min} and R_{max} obtained from the fits are listed in Table 2. For C_{10}TAB, R_{min} and R_{max} were found to be 0.1 and 4.4 Å, respectively. This implies that the diffusion of hydrogen atoms in a C_{10}TAB chain is restricted to spheres with radii between 0.1 and 4.4 Å. With increasing chain length, the radii of the spheres were found to decrease, and for C_{16}TAB, R_{min} and R_{max} were found to be 0.02 and 2.8 Å, respectively. However, with increasing temperature, the radii of the spheres increased, as shown in Table 2. It can be noted that the obtained values of R_{min} are very small, which indicates only that there is negligible mobility of the protons associated with the first carbon position near the headgroup, probably because of the inherent structure of the micelles. Similarly small values have been also reported for other systems.[23,33] A sketch to demonstrate the proposed model is shown in the inset of Figure 7, where the hydrogen atoms belonging to the headgroup perform a 3-fold jump rotation on a circle and the hydrogen atoms in the hydrophobic alkyl chain are shown to diffuse within spherical volumes of different sizes increasing linearly from the head to the tail.

The diffusivities associated with the different hydrogen atoms belonging to a C_nTAB monomer can be obtained from the $\Gamma_{in}(Q)$ values. These $\Gamma_{in}(Q)$ values were obtained by subtracting $\Gamma_G(Q)$ (width of the first Lorentzian) from the hwhm of the second Lorentzian, $\Gamma_{tot}(Q)$ (in eq 6) and are shown in Figure 8 for different C_nTAB micelles at 300 K. At

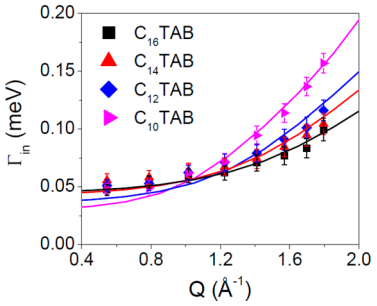

Figure 8. Variation with Q of the hwhm, Γ_{in}, of the Lorentzian $L_{in}(\Gamma_{in},\omega)$, corresponding to the internal motion of the monomer for C_nTAB micelles for different chain lengths at 300 K.

lower Q values, which essentially corresponds to motion at larger distances, $\Gamma_{in}(Q)$ was found to be independent of Q. This is a clear signature of localized diffusion in a confined region. The localized nature of this diffusion can be explained in terms of steric hindrance between the stacked molecules in the micelles. Because it is not possible to obtain an analytical expression for the hwhm of the quasielastic part for the present

dx.doi.org/10.1021/jp304841a | J. Phys. Chem. B 2012, 116, 9007−9015

model, one can calculate the hwhm numerically for given values of R_{min}, R_{max}, τ, D_{min}, and D_{max} using eqs 8, 9, 11, and 12. The least-squares fitting method was used to describe the observed QE width correspond to internal dynamics with τ, D_{min}, and D_{max} as parameters, whereas the values of R_{min} and R_{max} were already determined from the fits of the EISFs (Figure 7). The obtained values of τ, D_{min}, and D_{max} for different chain lengths are reported in Table 2.

The effects of chain length on the size, shape, aggregation number, and fractional charge of micelles have been very well studied and reported in the literature.[4−6] The various structural parameters of C_nTAB micelles having different chain lengths as obtained from SANS experiments by Berr[5] are listed in Table 1. The aggregation number increases dramatically with increasing chain length in these micelles. On the other hand, the fractional charge decreases with increasing chain length. The variations of the lengths of the major and minor axes indicate that a deformation from spherical to ellipsoidal is more dominant for the higher-chain-length systems. These observations have been explained in terms of an increase in the condensation of counterions on the micelles with increasing chain length of the monomer, as is evident from the fractional charges on the different micelles. The increased concentration of bound counterions screens electrostatic headgroup repulsions and allows the headgroups to move closer to each other. This, in turn, increases the packing density of the monomers within the micelles. Therefore, for C_{16}TAB (n = 16) micellar solutions, there is less space available between monomers than for C_{10}TAB (n = 10) micellar solutions. Increased packing of the monomers also results in the removal of water molecules within the micelles, and thus, the micelles become drier as the chain length increases. Hydration is known to influence the dynamics strongly in the cases of proteins, reverse micelles, and macromolecules.[16,27]

Our QENS results show that internal motions become hindered with increasing chain length (see Table 2): The diffusion coefficients decrease, and the volumes of the sphere within which the hydrogen atoms move are reduced. This can be explained in terms of an increased monomer packing density in micelles with longer chains, as discussed earlier. In C_{10}TAB micellar solution, hydrogen atoms are allowed to cover a larger volume with higher diffusivity compared to those in C_{16}TAB micellar solution. Therefore, with increasing monomer chain length, the flexibility of the chains in the micelles reduces, and the chains perform slower segmental motions. These results are also in agreement with those of a Raman scattering study of C_nTAB micellar solutions, which showed that the fraction of trans/gauche conformations in alkyl chains of C_nTAB increases with increasing alkyl-chain length, indicating a higher degree of conformational order.[14] An NMR study on C_nTAB aqueous solutions (n = 6, 8, 10, and 12) revealed that the limiting intradiffusion coefficient of the C_nTAB surfactant cation decreases with increasing chain length.[7] A recent MD simulation study[25] on SDS and SDBS micelles showed that the dodecyl chains of SDBS micelles are more tightly packed than those of SDS micelles, resulting in slower internal mobility in SDBS micelles. As shown in Table 2, the QENS results also indicate that, as the chain length increases, the 3-fold rotation of CH_3 units belonging to the headgroup gets slower. This can be explained in terms of the reduction of the Stern layer thickness.[5] Finally, as shown in Table 2, for C_{14}TAB micelles, the radii of the spheres and the associated diffusivities increase with temperature. As the temperature is increased, the monomers pack more loosely in the micelles as the distance between two consecutive monomers increases due to thermal energy. This, in turn, provides more free space and increased mobility of hydrogen atoms. Therefore, with increasing temperature, the alkyl chains become more flexible and perform faster internal motions.

CONCLUSIONS

The effects of chain length on the dynamics of C_nTAB micelles (n = 10, 12, 14, and 16) have been studied using high-resolution quasielastic neutron scattering. A model in which the micelles undergo global motion and monomers of the micelles perform internal dynamics successfully describes the observed dynamics of C_nTAB micelles. Diffusivity corresponding to the global motion was found to decrease with increasing chain length. This is explained in terms of the combined effects of increases in the hydrodynamic size and aggregation number of the micelles with increasing chain length. The proposed model of internal dynamics of C_nTAB micelles comprised two different components: segmental motion of the monomers and reorientation of the CH_3 units belonging to the headgroups. The residence time corresponding to 3-fold jump rotation of the headgroup was found to increase with increasing chain length, possibly because of a thinner Stern layer. The segmental motion of the monomers can be very well described by a localized translational diffusion model in which the hydrogen atoms in the alkyl chains perform diffusion within spherical volumes whose sizes increase linearly from head to tail. It was found that the hydrogen atoms in the alkyl chains in micelles with shorter chains are allowed to cover a larger volume with larger diffusivity than those in micelles with longer chains. This can be explained in terms of increased packing density of the monomers in the micelles with longer chains. The same model can also successfully describe the observed dynamical features at different temperatures in a consistent fashion.

In summary, the present work provides a consistent description of the dynamics in C_nTAB micellar solutions for surfactant molecules with varied chain lengths.

AUTHOR INFORMATION

Corresponding Author

*E-mail: mukhop@barc.gov.in. Tel.: +91-22-25594667. Fax: +91-22-25505151.

Notes

The authors declare no competing financial interest.

ACKNOWLEDGMENTS

We gratefully acknowledge Dr. P. A. Hassan, Chemistry Division, Bhabha Atomic Research Centre, for fruitful discussions. We also gratefully acknowledge access to the ISIS facility, STFC, U.K.

REFERENCES

(1) Rosen, M. J. *Surfactants and Interfacial Phenomena*; John Wiley & Sons: New York, 2004.
(2) Chevalier, Y.; Zemb, T. *Rep. Prog. Phys.* **1990**, *53*, 279−371.
(3) Jonsson, B.; Lindman, B.; Holmberg, K.; Kronberg, B. *Surfactants and Polymers in Aqueous Solution*; John Wiley & Sons: New York, 1998.
(4) Aswal, V. K.; Goyal, P. S. *Chem. Phys. Lett.* **2003**, *368*, 59−65.
(5) Berr, S. S. *J. Phys. Chem.* **1987**, *91*, 4760−4765.
(6) Joshi, J. V.; Aswal, V. K.; Goyal, P. S. *J. Macromol. Sci. B* **2008**, *47*, 338−347.

(7) D'Errico, G.; Ortona, O.; Paduano, L.; Vitag, V. *J. Colloid Interface Sci.* **2001**, *239*, 264−271.
(8) Roberts, M. F.; Redfield, A. G. *J. Am. Chem. Soc.* **2004**, *126*, 13765−13777.
(9) Bratt, P. J.; Gillies, D. G.; Sutcliffe, L. H.; Williams, A. J. *J. Phys. Chem.* **1990**, *94*, 2727−2729.
(10) Soderman, O.; Carlstrom, G.; Olsson, U.; Wong, T. C. *J. Chem. Soc., Faraday Trans.* **1988**, *84*, 4475−4486.
(11) Belmajdoub, A.; Elbayed, K.; Brondeau, J.; Canet, D.; Rico, I.; Lattes, A. *J. Phys. Chem.* **1988**, *92*, 3569−3573.
(12) Bockstaele, M. V.; Gelan, J.; Martens, H.; Put, J.; Schryver, F-C. D.; Dederen, J. C. *Chem. Phys. Lett.* **1980**, *70*, 605−609.
(13) Haramagatti, C. R.; Islamov, A.; Gibhardt, H.; Gorski, N.; Kuklin, A.; Eckold, G. *Phys. Chem. Chem. Phys.* **2006**, *8*, 994−1000.
(14) Haramagatti, C. R. Structure, Dynamics and Phase Behaviors of Cationic Micellar Solutions: Raman and Neutron Scattering Study of Alkyltrimethylammonium Bromides. *Doctoral Thesis*, Georg-August-Universität zu Göttingen, Göttingen, Germany, 2006.
(15) Bée, M. *Quasielastic Neutron Scattering: Principles and Applications in Solid State Chemistry, Biology and Materials Science*; Adam Hilger: Bristol, U.K., 1988.
(16) Freda, M.; Onori, G.; Paciaroni, A.; Santucci, A. *Phys. Rev. E* **2003**, *68*, 021406−7.
(17) Castelletto, V.; Hamley, I .W.; yang, Z.; Haeussler, W. *J. Chem. Phys.* **2003**, *119*, 8158−8161.
(18) Sharma, V. K; Mitra, S.; Verma, G.; Hassan, P. A.; Garcia Sakai, V.; Mukhopadhyay, R. *J. Phys. Chem. B* **2010**, *114*, 17049−17056.
(19) Sharma, V. K.; Mitra, S.; Verma, G.; Hassan, P. A.; Garcia Sakai, V.; Mukhopadhyay, R. *AIP Conf. Proc.* **2011**, *1349*, 995−996.
(20) Sharma, V. K.; Gunjan Verma, S.; Gautam, P. A.; Hassan, S.; Mitra; Mukhopadhyay, R. *Z. Phys. Chem.* **2010**, *224*, 253−261.
(21) Gerelli, Y.; Garcia Sakai, V.; Ollivierd, J.; Deriuab, A. *Soft Matter* **2011**, *7*, 3929−3935.
(22) Mitra, S.; Sharma, V. K.; Garcia Sakai, V.; Peter Embs, J.; Mukhopadhyay, R. *J. Phys. Chem. B* **2011**, *115*, 9732−9738.
(23) Doxastakis, M.; Garcia Sakai, V.; Ohtake, S.; Maranas, J. K.; de. Pablo, J. J. *Biophys. J.* **2007**, *92*, 147−161.
(24) Alexander, D.; MacKerell, Jr. *J. Phys. Chem.* **1995**, *99*, 1846−1855.
(25) Palazzesi, F.; Calvaresi, M.; Zerbetto, F. *Soft Matter* **2011**, *7*, 9148−9156.
(26) Böker, J.; Brickmann, J.; Bopp, P. *J. Phys. Chem.* **1994**, *98*, 712−717.
(27) Perez, J.; Zanotti, J. M.; Durand, D. *Biophys. J.* **1999**, *77*, 454−469.
(28) Gibrat, G.; Assairi, F. L.; Blouquit, Y.; Craescu, C. T.; Bellissent-Funel, M.-C. *Biophys. J.* **2008**, *95*, 5247−5256.
(29) Howells, W. S.; Garcia Sakai, V.; Demmel, F.; Telling, M. T. F.; Fernandez-Alonso, F. *The MODES User Guide*, version 3; Rutherford Appleton Laboratory: Didcot, U.K., 2010.
(30) Azuah, R. T.; Kneller, L. R.; Qiu, Y.; Tregenna-Piggott, P. L. W.; Brown, C. M.; Copley, J. R. D.; Dimeo, R. M. *J. Res. Natl. Inst. Stan. Technol.* **2009**, *114*, 341−358.
(31) Carpentier, L.; Bée, M.; Giroud-Godquin, A. M.; Maldivi, P.; Marchon, J. C. *Mol. Phys.* **1989**, *68*, 1367−1378.
(32) Volino, F.; Dianoux, A. J. *Mol. Phys.* **1980**, *41*, 271−279.
(33) Trapp, M.; Gutberlet, T.; Juranyi, F.; Unruh, T.; Demé, B.; Tehei, M.; Peters, J. *J. Chem. Phys.* **2010**, *133*, 164505.